Extreme diversity of phage amplification rates and phage-antibiotic interactions revealed by PHORCE

Yuval Mulla[1,2,*,‡], Janina Müller[1,*], Denny Trimcev[1], and Tobias Bollenbach[1,3,‡]

1. Institute for Biological Physics, University of Cologne, 50931 Cologne, Germany
2. Molecular Microbiology Section, A-LIFE, AIMMS, Vrije Universiteit, 1081 BT Amsterdam, The Netherlands
3. Center for Data and Simulation Science, University of Cologne, 50931 Cologne, Germany

* These authors contributed equally.

‡ Correspondence: y.mulla@vu.nl, t.bollenbach@uni-koeln.de

Abstract

Growth rate plays a fundamental role in microbiology and serves as an important proxy for fitness in evolution. While high-throughput measurements of bacterial growth rates are easily performed in any microbiology lab, similar methods are lacking for phages. This gap hinders systematic comparisons of important phage phenotypes, such as their amplification rate in bacterial populations and their bactericidal effect, across different phages and environmental conditions. Here, we show that the amplification rate of lytic phages can be readily quantified by analyzing bacterial population growth and collapse dynamics under phage predation using a parsimonious mathematical model – an approach termed PHORCE (Phage-Host Observation for Rate estimation from Collapse Events). The resulting phage amplification rate captures the bactericidal effect independent of initial phage and bacterial population sizes and across different growth conditions. Using high-throughput PHORCE, we found that the amplification rates of *Escherichia coli* phages vary widely by more than three orders of magnitude. Furthermore, our approach shows that phage–antibiotic interactions are predominantly determined by the antibiotic, and not by the phage. In particular, the ribosome-inhibiting antibiotic doxycycline generally showed antagonism with phage amplification, while the DNA-damaging antibiotic nitrofurantoin proved synergistic. This framework provides a means to quantitatively characterize phage phenotypes and may facilitate future high-throughput phage screens for antibacterial applications.

Introduction

Advances in metagenomic sequencing have revealed a staggering genomic diversity of phages[1]. A major challenge now is to understand how these diverse phages affect microbial communities, particularly through their ability to kill their bacterial hosts. While there are standardized measures of antibiotic activity, such as the minimal inhibitory concentration (MIC)[5], a similar metric for measuring the antibacterial activity of phages is lacking. This is a

pressing problem for potential applications of phages in therapeutics, the success of which depends on the bactericidal effect of phages[2–4]. This problem extends to the assessment of phage–antibiotic combinations. Indeed, a recent retrospective study showed that phage-antibiotic synergy (PAS) is critical for the success of phage therapies[5]. The identification of synergistic combinations has particular potential, but due to the lack of quantitative measures of phage activity, there is no consensus quantitative definition of phage–antibiotic synergy. This situation limits a rigorous comparison between treatment options. Clearly, new approaches to quantify phage activity, ideally in high throughput, are urgently needed.

While bacterial population size can be monitored dynamically during growth via optical density, phages must be isolated from their hosts at each time point before quantification[6–8] to determine their kinetic properties[9]. Genomically encoded fluorescence could solve this problem, but is challenging to engineer non-invasively in phages and is rarely used. A promising approach to circumvent this problem is to use growth curves in phage predation assays (Fig. 1a) to infer phage amplification parameters (burst rate, adsorption rate, and burst size, Fig. 2c) via mechanistic mathematical models[7,10,11]. However, these approaches still rely on time-resolved measurements of phage concentrations[7,10,11], which severely limits throughput. By contrast, several empirical quantifications of phage activity depend only on bacterial growth curves[12–16]. While phage predation experiments are relatively straightforward, commonly used ad hoc measures (e.g. the area under the growth curve[16]) are sensitively dependent on the initial phage and bacterial concentrations. Therefore cumbersome and error-prone normalization steps are required to enable meaningful comparisons between experiments[17]. Such ad hoc measures are particularly difficult to interpret when comparing phage activity at different bacterial growth rates[17]. As a result, rigorous quantification of phage activity at inhibitory, and therefore clinically relevant, antibiotic concentrations remains a challenge[18].

Here, we present PHORCE, a new approach to determine the phage amplification rate in dependence of the bacterial concentration directly from bacterial growth curves. This approach allows us to study the phenotypic diversity of lytic phages and to detect phage-antibiotic interactions. We show that the phage amplification rate is a phage-intrinsic kinetic property in that it is insensitive to the initial phage and bacterial concentrations. Importantly, the approach does not require time-resolved phage concentration measurements, opening the door to high-throughput applications. We illustrate the power of PHORCE by measuring amplification rates for the entire BASEL collection of *Escherichia coli* phages[19], revealing that they differ by more than three orders of magnitude and correlate with phage taxonomy. Finally, we show how PHORCE allows for a rigorous definition of phage–antibiotic interactions based on the antibiotic dependence of the phage amplification rate.

Results

PHORCE captures phage-host dynamics

We aimed to quantitatively understand the dynamics of a phage population in a growing bacterial population. To use an assay that could be readily scaled up, we infected an exponentially growing culture of *E. coli* with a lytic phage (Bas04, a highly active lytic phage

from a publicly available phage library[19]) and measured bioluminescence over time as a proxy for bacterial concentration (Fig. 1a). We tracked population size using bioluminescence rather than optical density because both are proportional to biomass at steady state, but bioluminescence provides a superior signal-to-noise ratio[20]. Indeed, both read-outs report similar dynamics (Suppl. Fig. 1). We observed that the initial growth of bacteria with and without phages is similar, in particular exhibiting the same growth rate (Fig. 1a). This is in contrast to most antibiotics, which rapidly decrease the bacterial growth rate at sufficient concentrations. However, after eight hours, the bacterial population suddenly collapsed in the presence of phage (orange), while the no-phage control (blue) maintained its exponential growth. This sudden collapse, which has been observed in many previous studies using lytic phages[12–14], is due to phage predation and therefore depends on the bactericidal effect of a phage: At the time of collapse, the phage population is large enough to lyse bacteria at a higher rate than they can grow.

Successful phage predation consists of two critical steps: First, a phage adsorbs to the bacterial host. After a delay required for phage replication within the host, the second step occurs: The bursting of the infected bacterium and the release of phage particles. To model this process, we first investigated which of these two steps (adsorption or bursting) is rate-limiting for the infection cycle under our conditions. Importantly, the adsorption rate depends on the bacterial concentration, whereas the burst rate typically does not. We reasoned that this distinction could be exploited to identify the rate-limiting step in our assay: If only bursting is limiting, then the collapse time should be independent of absolute concentration (Supplementary Information). To test this directly, we used the growth curve assay to measure collapse times for a wide range of initial bacterial densities (Fig. 1b) while maintaining a fixed bacterium-to-phage ratio (multiplicity of infection, MOI). Instead of a constant collapse time, we observed a precise logarithmic decrease in collapse time with initial bacterial concentration over three orders of magnitude (Fig. 1b, c). These results indicate that, under our conditions, adsorption is rate-limiting for the phage infection cycle (Supplementary Information).

Trying to quantitatively explain our observations, we analyzed a minimal mathematical model of phage predation[11] (Fig. 2c). The model consists of coupled differential equations to describe bacterial growth and phage-induced death and phage replication (Supplementary Information). In the regime of adsorption-limited phage predation, we derive an analytical result for the collapse time t_{col} (Supplementary Information):

$$t_{\mathrm{col}} = \frac{1}{r_{\mathrm{bac}}} \log\left(1 + \frac{r_{\mathrm{bac}}}{r_{\mathrm{pha}} b_0} \log\left(\frac{p_\infty}{p_0}\right)\right) \tag{1}$$

Here, $r_{\mathrm{pha}} = n_{\mathrm{burst}} k_{\mathrm{adsorp}}$ is the product of the adsorption constant k_{adsorb} and the burst size n_{burst} (Supplementary Information), which plays the role of an amplification rate for phages in the adsorption-limited regime (see below). p_0 and p_∞ denote the initial and final phage concentrations, respectively, b_0 is the initial bacterial concentration, and r_{bac} is the bacterial growth rate. Note that mathematically, the product of r_{pha} and the bacterial concentration gives a specific population growth rate, analogous to the well-established bacterial growth rate. In essence, r_{pha} quantifies how fast the phage population can grow in a bacterial population and conveniently characterizes the double-exponential amplification of

phages in an exponentially growing bacterial population, regardless of the bacterial concentration. Therefore, we refer to r_{pha} simply as the *phage amplification rate*. Unlike parameters previously used to characterize phage amplification, the phage amplification rate thus defined is independent of bacterial and phage concentrations[12–14,17].

Our result for the collapse time (Eq. 1) provides an efficient way to test whether the mathematical model is consistent with the dynamics observed in phage predation experiments. To this end, we next performed experiments in which we systematically varied initial bacterial densities over two orders of magnitude (Fig. 2a-b, colors) and initial phage densities over three orders of magnitude (Fig. 2a, columns) and quantified the collapse times for the two-dimensional array of all 80 pairwise combinations. Next, we estimated the fold increase in phage population size p_∞/p_0 from subsequent measurements of bacterial growth curves (Ref. [7], Methods, Suppl. Fig. 2). This rich quantitative dataset allows a powerful test of the model's prediction of collapse time, since the phage amplification rate remains as the sole free parameter in Eq. 1. We found a quantitative agreement between the model and the experimental data over the entire range of initial conditions for a single value of the phage amplification rate (Fig. 2d, ρ=0.9). These results support that the mathematical model faithfully captures the essence of the phage predation dynamics over several orders of magnitude of initial phage and bacterial densities – up to the point of collapse (post-collapse dynamics are beyond the scope of this model). While the rate of bursting may also contribute to the dynamics, assuming adsorption as the sole rate-limiting step already quantitatively explains our results. This approach also illustrates that the phage amplification rate can be readily measured without the need for considerably more laborious time-resolved measurements of phage concentration[7,11,21]. We call this approach for quantifying phage amplification rates PHORCE (Phage-Host Observation for Rate estimation from Collapse Events).

Phage amplification rates show great diversity

To test the broader applicability of PHORCE, we applied it to the entire BASEL collection of 69 different lytic *E. coli* phages[19] (Fig. 3a). These phages are ideally suited for this purpose because they all infect the *E. coli* strain used in this study, are thought to represent natural *E. coli* phage diversity, and are well characterized phenotypically and genetically[19]. Bacterial growth curves for similar initial phage and bacterial densities showed that the collapse time is strongly dependent on the phage used, as expected (Fig. 3b, Suppl. Fig. 3). We confirmed the main observations made above with the Bas04 phage (Fig. 1-2): The collapse time generally decreases with the initial bacterial concentration at a fixed multiplicity of infection (Suppl. Fig. 4a), and the minimal model of phage predation in the adsorption-limited regime faithfully captures the dynamics for the entire BASEL collection using the phage amplification rate as the sole fit parameter (Suppl. Fig. 4b). These results demonstrate that PHORCE is applicable to diverse lytic phages and can be readily used as a method for quantifying phage amplification rates in high-throughput assays.

Applying PHORCE to all phages in the BASEL collection revealed an enormous diversity of phage amplification rates. These rates varied by more than three orders of magnitude among the phages (Fig. 3c), and the true diversity is even greater because some phage amplification rates were below the detection limit of our technique. To put this diversity into perspective, the amplification rates of the host of these phages (i.e., different *E. coli* strains)

vary by less than an order of magnitude in common growth media, and even the growth-rate ratio between the fastest-growing known bacterium, *Vibrio natriegens*, and the notoriously slow-growing *Mycobacterium tuberculosis* is more than ten times smaller than the observed range of phage amplification rates. We expect the diversity of phage amplification rates to increase even further when other bacterial hosts are considered.

We found that the phage genus partially determines the phage amplification rate. In particular, *Vequintavirus* members amplify significantly slower than other phages ($p=3\times10^{-4}$, Fig. 3d). However, we did not find any relationship between amplification rate and other phage characteristics, such as genome size or primary/terminal receptor. Of particular interest is phage morphology, which has traditionally been used to classify phages. In contrast to the phage genus, phage morphology had no predictive value for phage amplification rate (Suppl. Fig. 4c). This lack of association between morphology and phenotype further supports the plausibility of the modern phage classification based on sequence rather than morphology.

How does the phage amplification rate compare to other measures of phage efficacy? A common measure of phage efficacy is the total number of phages present in the culture at the end of a phage predation experiment, e.g. determined by a plaque assay[22,23]. While this phage yield is clearly distinct from the phage amplification rate, it is possible that in practice these two quantities are highly correlated and measure essentially the same underlying property. We have already shown that the phage amplification rate faithfully captures the collapse time of bacterial populations across a wide range of initial conditions (Fig. 2d, Suppl. Fig. 4b), but phage yield did not correlate at all with this key quantity (Suppl. Fig. 4d). These results suggest that, in addition to conceptual advantages such as independence of initial phage and bacterial densities, phage amplification rate can be a useful measure to quantify phage efficacy for potential therapeutic applications aimed at eradicating bacterial populations.

Phage-antibiotic interactions are largely determined by antibiotics

Since PHORCE can disentangle phage amplification rates from bacterial growth rates, we reasoned that it could be suitable for characterizing interactions between phages and antibiotics. Antibiotics can interfere with the ability of phages to infect bacteria; a case in point are aminoglycosides which have recently been shown to be potent inhibitors of phage infection[23]. Our approach should readily detect such phage-antibiotic interactions, which are analogous to drug interactions[20]. A key difference is that drug interactions between antibiotics are typically defined in terms of the drugs' quantitative effects on the bacterial growth rate[20]. This approach is not directly applicable to phage-antibiotic interactions, because phages do not simply lead to exponential growth with a lower rate, but rather to more complicated population dynamics (Fig. 1). In a plausible definition of phage–antibiotic interactions, antagonism leads to a decrease in phage amplification rate in the presence of the antibiotic and synergy to an increase; in a neutral interaction, the antibiotic does not affect the phage amplification rate. The fact that the phage amplification rate is independent of initial conditions and easy to measure is valuable for the rigorous definition and quantification of phage-antibiotic interactions.

To test this idea, we measured phage amplification rates in the presence of antibiotics at different concentrations. We first focused on the phage Bas04 and a fine-resolution concentration gradient of the ribosome-inhibiting antibiotic doxycycline. The phage-induced collapse time showed a clear monotonic increase with doxycycline concentration, while the bacterial population size (measured by luminescence intensity, see Methods) at which the collapse occurred remained nearly constant upon drug addition (Fig. 4b). The phage amplification rate derived from these data (Suppl. Eq. 6) decreased with increasing antibiotic concentration (Fig. 4c, blue), revealing a clear antagonistic interaction between Bas04 and doxycycline. This antagonism is not a general consequence of lowering the bacterial amplification rate because the interaction of this phage with the DNA-damaging drug nitrofurantoin is strikingly different: Here, the collapse time remained nearly constant and the magnitude of the collapse rapidly increased with drug concentration. The phage amplification rate increased monotonically with the drug concentration (Fig. 4a,c, orange), revealing a clear case of synergy between Bas04 and nitrofurantoin. These results show that antibiotics can drastically affect phage amplification in a synergistic or antagonistic manner, which can be detected using PHORCE.

To determine whether the observed interactions between antibiotics and phages are specific to each phage or reflect more general effects of the drugs on phage infection, we analyzed phage–antibiotic interactions for a diverse selection of phages. We measured the amplification rate of nine different phages from the BASEL collection in fine-resolution concentration gradients of nitrofurantoin and doxycycline. Similar to Bas04 above, these experiments showed clear effects of the antibiotics on the dynamics of bacterial population collapse for most phages (Suppl. Fig. 5). To systematically detect phage-antibiotic interactions, we analyzed the correlation between phage amplification rate and drug concentration for each phage-antibiotic combination (Fig. 4c-d). Since we do not know the functional form (e.g., linearity) of the antibiotic-dependent phage amplification rate, we used Kendall's τ as the interaction score, with $\tau > 0$ indicating synergy, and $\tau < 0$ antagonism, and $p < 0.05$ as the significance threshold. The interaction score strictly identifies only the direction (synergy or antagonism), but we found that it correlates with the strength of the interaction (Kendall's τ=0.5 , p=0.002, Suppl. Fig. 6a).

For doxycycline, this analysis revealed four cases of neutrality (p<0.05) and no case of synergy; the majority of interactions (5 out of 9) were antagonistic (Fig. 4e-f). In contrast, the majority of phages (6 out of 9) showed synergy with nitrofurantoin while not a single case of antagonism was detected for this drug (Fig. 4e-f). Thus, phages that showed any interaction at all generally synergized with nitrofurantoin but were antagonized by doxycycline. Additionally, the interaction scores for both drugs were not correlated across different phages (Kendall's τ=0.1, p=0.6; Fig. 4f). Taken together, these results indicate that phage-antibiotic interactions are primarily determined by the antibiotic and less by the phage.

Previous studies of phage-antibiotic interactions have mostly focused on synergy and often relied on endpoint measurements of phage yield[22,23]. We tested the extent to which these methods correlate with our approach, which is based on the dynamics of bacterial population growth and collapse. While there is a clear difference in the bacterial growth curves between nitrofurantoin and doxycycline for Bas04 (Fig. 4a–c), the phage yield decreases similarly with increasing concentration for both antibiotics (Fig. 4d). In fact, we found no correlation between the antibiotic-dependence of phage yield and the antibiotic-dependence of phage

amplification rate across all phages and drug concentrations for both antibiotics (Kendall's τ =0.05, p=0.9, Suppl. Fig. 6b). Together with the lack of correlation between phage amplification rate and phage yield across the entire BASEL collection (Suppl. Fig. 4d), these results show that the phage amplification rate is a distinct property of phages that is largely independent of the commonly used phage yield. While endpoint measurements of phage yield are certainly relevant in other contexts, the phage amplification rate quantitatively captures the bactericidal effect of phages across diverse conditions (Fig. 2d, Suppl. Fig. 4b) and is thus a key quantity relevant to phage-antibiotic synergy.

Discussion

We have shown that phage amplification under our conditions is primarily limited by phage–bacteria adsorption (Fig. 1), allowing characterization of phage bactericidal effect by a single parameter, the phage amplification rate. The phage amplification rate is readily measured with PHORCE and insensitive to the initial phage and bacterial concentrations (Fig. 2). Applying PHORCE to the entire BASEL collection of diverse *E. coli* phages revealed that the phage amplification rate varies by more than three orders of magnitude (Fig. 3). Using the phage amplification rate to quantitatively characterize phage-antibiotic interactions, we observed that doxycycline antagonized many phages, while nitrofurantoin often synergized with them (Fig. 4).

Similar to the specific growth rate of bacteria, which is one of the cornerstones of microbiology, phage amplification rate provides a key phage characteristic that can be directly compared across different phages, hosts, and growth conditions. This is difficult to achieve with empirical quantifications[12–14,17]. While plaque size measurements have been used to detect bactericidal effect[24], they are hard to standardize across experiments and laboratories due to their sensitivity to initial conditions[25]. In addition, PHORCE does not require time-resolved measurements of phage concentrations, resulting in greatly increased throughput compared to previous mechanistic models[7,10,11]. Previous studies on phage-antibiotic synergy have often relied on the phage yield[22,23], which does not correlate with bactericidal effect under our conditions (Suppl. Fig. 4d, Suppl. Fig. 6b). Instead, we propose to use the phage amplification rate as the primary measure of a phage's bactericidal effect, similar to how the Minimal Inhibitory Concentration (MIC) is used to assess the bactericidal effect of antibiotics.

The enormous diversity in phage amplification rates we observed (Fig. 3) has a number of implications. Phages play a vital role as bacterial predators in various ecosystems such as the ocean, gut, and soil, for which recent studies have extensively characterized phage-host networks of infectivity[26–28]. Our findings highlight large variation in bactericidal effect among phages. This implies that phage-host interactions occupy a continuum of activity, rather than the simple binary yes–no classification often used[26–28]. This continuum of phage activity also has potential implications for phage therapy. While some personalized phage therapies consider quantitative measures of bactericidal effect[29], off-the-shelf cocktails typically rely on binary measures of phage-host interactions[30–32], in part due to a lack of easy-to-use techniques for comparing phage activity across hosts. This is a missed opportunity, as highlighted by a strong correlation between phage amplification rate and therapeutic efficacy recently observed in a *Drosophila melanogaster* infection model[18]. Measuring phage amplification rates has traditionally required laborious time-resolved measurements of phage

concentration[4]. Our high-throughput approach eliminates the need for such time-consuming measurements, using standard equipment that can be seamlessly integrated into product development pipelines.

Using PHORCE, we observed a notable pattern: Phage–antibiotic interactions are more strongly determined by the antibiotic rather than by the phage itself (Fig. 4e-f). This suggests a mechanism whereby antibiotics have a broad effect on the ability of phages to replicate inside bacterial cells. For example, doxycycline inhibits ribosomes[20], which likely stops phage production because phages cannot hijack them as usual[33]. This could explain the widespread antagonism observed with doxycycline (Fig. 4). Nitrofurantoin's mechanism of action is more intricate and involves the reduction of this prodrug to reactive intermediates that damage various cellular components; ultimately, resulting in decreased transcription[6]. We speculate that this reduced transcription and subsequent reduced load on the protein synthesis machinery may facilitate phage replication by hijacking this machinery. Investigating the underlying mechanisms of phage–antibiotic interactions is an interesting avenue for future work. As a starting point, it would be valuable to explore whether phage–antibiotic interactions are generally determined by the drug's mode of action, by extending the approach presented here to measure a comprehensive phage-antibiotic interaction network for a wider range of phages and a diverse set of antibiotics.

Our approach has applications beyond phage–antibiotic interactions and phage cocktail design. Phages are typically classified as generalists or specialists based on their ability to infect a wide or narrow range of hosts, respectively[35]. A fundamental question is whether generalism is associated with a fitness cost. Measurements of phage amplification rate are well suited to directly address such fitness tradeoffs. Since amplification rate is a key aspect of phage fitness, we see another application of PHORCE in evolutionary biology. Phages, with their large numbers, short generation times, and compact genomes are a popular model system in laboratory evolution[36]. While their evolution is nowadays relatively easy to characterize genotypically, there is a lack of quantitative methods to assess their phenotypic evolution. PHORCE can fill this gap. Finally, the unprecedented ease with which phage amplification rates can be measured opens up the possibility of systematically investigating quantitative relationships between these amplification rates and various aspects of phage and bacterial physiology. This may lead to the discovery of phage amplification laws analogous to bacterial growth laws[37].

Materials and Methods

Bacterial strains and bacteriophages

All collapse curve experiments were performed with *E. coli* K-12 BW25113 transformed with a kanamycin-resistance-bearing plasmid (pCS-λ) carrying luciferase genes used to determine the growth rate[20]. The two-dimensional (2D) gradient experiments (Figs. 1-2, Suppl. Fig. 1-2) employed the Bas04 bacteriophage, sourced from the BASEL collection[19]. For the antibiotic-phage interactions (Fig. 4, Suppl. Fig. 5-6), a subset of nine phages (Bas01; Bas04; Bas10; Bas14; Bas23; Bas30; Bas37; Bas42; Bas63) was chosen to represent a wide diversity of phage amplification rates and phage families. Additionally, *E. coli* K-12 MG1655 ΔRM, an isolation strain from the BASEL collection, was used for conducting plaque assays to determine phage titers and for the generation of phage stock solutions. Purified phage stocks were stored at 4°C, whereas bacterial stocks were stored at -70°C with the addition of glycerol (17% in final solution). Both were stored in CryoPure tubes (Sarstedt, 72.377.992).

Growth media

For all collapse curve and reinoculation experiments, LB Broth Lennox medium (Sigma Aldrich, L3022) enriched with 5mM $MgSO_4$ (Sigma Aldrich, M7506) was utilized. The plaque assays employed the double agar overlay assay (DAOA) technique[6], which required an underlay of 1.5% LB agar (Sigma Aldrich, L2897) and an overlay of 0.5% LB agar, both supplemented with 5mM $MgSO_4$. In the DAOA process, bacterial overnight culture (ONC) was added to the overlay to an optical density (OD) of 0.4 within the soft agar.

To produce spent medium for the dilution and storage of phage stocks, an overnight culture of *E. coli* MG1655 pCS-λ, ranging from 15 to 20 ml, was centrifuged at 3260 × *g* for 30 to 40 minutes using a standard 50 ml Falcon tube (Sarstedt, 62.547.254). The supernatant was then passed through a 0.2 µm syringe filter (Corning, CLS431227) and stored at 4°C for subsequent use.

The antibiotics used were doxycycline (Sigma Aldrich, D9891) and nitrofurantoin (Sigma Aldrich, N7878). The doxycycline stock solution was prepared by dissolving it in DMSO (Sigma Aldrich, D8418), while nitrofurantoin was dissolved in DMF (Sigma Aldrich, D4551). Both solutions were then filter-sterilized and stored at −20°C in the dark. Aliquots were thawed at room temperature before use.

Two-dimensional gradient of initial phage and bacterial concentration

We prepared phage predation assays with a two-dimensional gradient of initial bacterial and phage concentrations (Fig. 2). To initiate the preculture, 2 ml of medium was inoculated with 4 µl of an ONC in a standard 10 ml glass test tube. This mixture was then incubated in a shaking incubator (Innova 44, Eppendorf New Brunswick, DE) at 30°C and 225 rpm for 2–3 hours. Subsequently, a gradient of phage titers was established in a 12-column deep well plate using a 1:2 serial dilution procedure, resulting in 6 ml per phage concentration. This prepared medium filled the 2nd to 8th row of a white, flat-bottom LumiNunc F96-MicroWell microtiter plate (Thermo Fisher Scientific, 732-2697). From there, 1185 µl of the medium was

transferred into a 12-channel reagent reservoir (Carl Roth, EKT4.1), and 15 µl of the preculture was added to each channel, followed by thorough mixing. To create a gradient of bacterial concentrations, 280 µl of this mixture was transferred to the top row of the microtiter plate, employing a 1:2 serial dilution down the columns of the plate. The assembled plate was sealed with a TopSeal-A Plus transparent foil (PerkinElmer, 6050185) and placed in a Synergy H1 plate reader (BioTek Inc., VT, USA) set at 30°C and 807 rpm. Here, bioluminescence was monitored every 5 minutes. Dual acquisition of both optical density and bioluminescence (Fig. 1, Suppl. Fig. 1) was achieved by performing experiments in black plates with a transparent bottom (CELLSTAR Ref. No 655087). Data points were acquired every 20 minutes. In addition, the cell density of the preculture was determined with a Coulter counter as described below.

Antibiotic gradients

We prepared phage predation assays for gradients of two different antibiotics, doxycycline and nitrofurantoin (Fig. 4, Suppl. Fig. 5-6). For both antibiotics, eight-concentration gradients were constructed using serial dilution (1:1.5 ratio). The highest concentration was set at 3.3 µg/ml for doxycycline and at 4 µg/ml for nitrofurantoin.
For doxycycline, 1.5 ml of medium of each antibiotic concentration was aliquoted into standard 10 ml glass test tubes. Bacterial overnight cultures (ONC) were inoculated into the concentration gradient from frozen stocks at dilutions ranging from 1:1500 to 1:3000. For nitrofurantoin, 1.5 ml of medium at each concentration was added to a 12-channel reservoir, followed by inoculation of bacterial ONC from a frozen stock at a 1:1500 dilution. This mixture was then distributed across two rows of a microtiter plate. For both antibiotics, bacterial precultures were then incubated at 30°C and 225 rpm (doxycycline) or 807 rpm (nitrofurantoin) in a shaking incubator for 4 hours.
Concurrently, phages from the BASEL collection were diluted 1:360 in spent medium. After incubation, 1350 µl of each bacterial preculture was mixed with 4.5 ml of medium for doxycycline concentrations. For nitrofurantoin, cultures from one row were adjusted to a uniform bioluminescence level. Additionally, 100 µl of each preculture was diluted in 12 ml Isotone for Coulter counter evaluation for both antibiotics.
138 µl of the resulting cultures were added to each well of a microtiter plate, ensuring that each row corresponded to a specific antibiotic concentration. Next, 2 µl of the phage dilution (1:360) was added to each column, standardizing the phage across columns, except for the last column, which was left phage-free as a control. The plates were sealed with transparent foil and incubated in a plate reader at 30°C and 807 rpm. Bioluminescence was monitored continuously every 5 minutes for 17 to 20 hours for both antibiotics. Note that the determination of collapse time is insensitive to any potential effect of the antibiotic on the bioluminescence signal per cell.

Phage purification

For phage purification, 130 µl of a phage-bacteria mixture was combined with 130 µl of medium and approximately 15 µl of chloroform (Sigma Aldrich, 372978) in each well of a 96-well deep well plate. The plate was then subjected to vigorous shaking at approximately 1200 rpm using a Titramax 1000 platform shaker (Heidolph, 544-12200-00) for a duration of 5 to 10 minutes. Following this, an additional 1040 µl of medium was introduced to each well, and the plate was shaken again, this time at a lower speed of 600 rpm, for 2 minutes to

ensure thorough mixing. In the next step, the plate was centrifuged at 2580 rpm for 30 to 40 minutes, aiming to sediment the cell lysate at the bottom of the wells. Post-centrifugation, 150 µl from the supernatant of each well was carefully transferred into a new 96-well microtiter plate. Due to the addition of medium during the purification process, the resulting product corresponds to a 1:10 dilution of the pure phage lysate.

Measurement of final phage concentrations

We measure final phage concentrations (Fig. 4d, Suppl. Fig. 4d) by purifying the product of the phage predation assays (see section “Phage purification”), reinoculating it with bacteria and comparing the collapse times with a dilution series of the respective phage stock. For initiating the bacterial preculture, 2 ml of medium was inoculated with 4µl of a frozen ONC stock in a standard glass test tube. This mixture was then incubated in a shaking incubator at 30°C and 225 rpm for 2-3 hours. Following incubation, the preculture was diluted in a range from 1:60 to 1:300 with fresh medium and aliquoted to a microtiter plate, dispensing 138.6 µl into each well. Each well then received 1.4 µl of either the phage purification product (at a 1:10 dilution) for reinoculation or an equivalent volume of fresh medium for control wells. To construct calibration curves, one column per phage strain was used, starting with a phage stock dilution of 1:100 in the top well and proceeding with a 1:3 dilution series down the column. The plate was subsequently sealed and bioluminescence was measured as described above.

Quantification of cell densities

For Coulter counter measurements, bacterial culture volumes ranging from 10 to 100 µl were diluted in 12 ml of Isotone II diluent in a Coulter counter cuvette (Beckman Coulter, 580015). The diluted samples were then vortexed at a medium speed. After vortexing, the samples were transferred to a Multisizer 3 Coulter counter (Beckman Coulter), equipped with a 10 µm aperture. The samples were allowed to stabilize for 1–2 minutes before initiating the measurement. In each measurement, a 500 µl sample is analyzed by the device.

Drop assay for stock concentrations of phage samples

Plates for the drop plaque assay were prepared using the Double Agar Overlay Assay (DAOA) technique (see section “Growth media”). First, the underlay medium was microwaved until liquefied and then cooled to 60°C, where it was held overnight. Subsequently, 38 ml of this medium was poured into an Nunc OmniTray single-well plate (Thermo Fisher Scientific, 242811) and left to dry under a laminar flow hood for 15 minutes. For the overlay, bacterial ONC was added to the overlay medium at 60°C, to achieve an OD of 0.4. Five ml of this mixture was then layered over the solidified underlay in the omnitray plate. Finally, phage samples were diluted in a 1:10 dilution series and 5 µl droplets from each dilution (10^{-5} to 10^{-9}) were carefully applied to the overlay using a MINI 96 electronic 96-channel pipette (Integra, 4803). Plaque-forming unit (PFU) counting was conducted manually for all dilutions where plaques did not overlap.

Analysis of bacterial growth curves

The bacterial growth rate was extracted from bioluminescence curves of bacterial cultures without phages. Curves were fitted in the range of $t>0.5$ h and bioluminescence $< 10^6$ AU. A

first order polynomial was fitted (Levenberg-Marquardt method implemented with Python's optimize.curve_fit, SciPy 1.11.1) to the bioluminescence values in log space to ensure that the low concentration part of the curve also contributed to the fit. The slope of the curve was taken as the bacterial growth rate, whereas the intersection was used to estimate the initial bacterial concentration (see below). The collapse time of phage predation curves was extracted by using Python's find_peaks (SciPy 1.11.1), using a width of four data points (20 minutes) for smoothing. Collapse points with bioluminescence values above 3×10^5 AU were excluded as they were outside of the steady state exponential growth regime. When multiple initial conditions were present of the same phage in the same growth conditions (Fig. 2d, Fig. 3c-d, Suppl. Fig. 4c-e), Eq. 1 was fitted using optimize.curve_fit, SciPy 1.11.1 to extract the phage amplification rate from multiple growth curves. Otherwise, the phage amplification rate was calculated from a single growth curve using:

$$r_{\mathrm{pha}} = r_{\mathrm{bac}} \frac{\log(p_\infty/p_0)}{b_0 \exp(t_{\mathrm{col}} r_{\mathrm{bac}}) - b_0} \tag{2}$$

r_{bac} was extracted from a bacterial growth curve in the absence of the phage, as described above. b_0 was measured using a Coulter counter. We determined the ratio p_∞/p_0 in a high throughput manner inspired by Ref. [7]: we purified the phage from the experiment of interest (e.g. in the presence of antibiotic), diluted it by a factor of d (typically 60-300) and added bacteria from a fresh stock to measure the collapse time. For each phage, we create a calibration curve by measuring the collapse time at various phage stock dilutions (p_{stock}/p_0) against the same fresh bacterial stock. We fit the calibration curve with the following equation:

$$t_{\mathrm{col,stock}} = a\ \log(p_{\mathrm{stock}}/p_0) + b \tag{3}$$

We then extract the relative phage concentration using:

$$\frac{p_\infty}{p_{\mathrm{stock}}} = e^{(t_{\mathrm{col}}-b)/a} d \tag{4}$$

Lastly, by multiplying $p_\infty/p_{\mathrm{stock}}$ with the dilution factor of the first growth experiment (p_{stock}/p_0), we obtain p_∞/p_0.

The standard errors of the phage amplification rate (Fig. 1c, 4c) and the phage concentration (Fig. 4d) were determined by bootstrapping the growth curves 1000× and determining the collapse time to estimate its standard deviation. This error was then propagated to either the phage amplification rate or the relative phage stock concentration (Eq. 2 or 4, respectively).

Notably, the phage amplification rate only logarithmically depends on $p_\infty/p_{\mathrm{stock}}$. Since the experimental determination of p_∞/p_0 is relatively laborious to perform for many phages simultaneously, even with the above method, we tested whether the phage amplification rate could be approximated by assuming $p_\infty/p_0 \approx p_{\mathrm{stock}}/p_0$. We tested this for nine different phages (Suppl. Fig. 5e) and found that this assumption gives very similar results to explicitly measuring p_∞/p_0 (Pearson's $\rho=0.95$, $p=10^{-22}$). Therefore, when measuring the amplification

rate of the entire BASEL collection (Fig. 2), we omitted the measurement of p_∞/p_0 and instead assumed $p_\infty/p_0 = p_{\text{stock}}/p_0$.

For the measurements of antibiotic-dependent phage amplification rates (Fig. 3, Suppl. Fig. 6) we had many different initial conditions. While plate reader experiments can be performed in high throughput on 96-well plates, measuring the initial bacterial concentration (b_0) required single sample Coulter counter experiments. Therefore, we measured to what extent the initial bioluminescence intensity of growth curves (see above) could replace the Coulter counter experiments. For a limited set of replicates (1×8 concentrations of nitrofurantoin and 2×8 concentrations of doxycycline) and nine different phages, we measured the phage amplification rate by measuring b_0 with the Coulter counter and p_∞/p_0 with subsequent bacterial growth curves. We compared the amplification rate determined from both of these measured parameters (abscissa, Suppl. Fig. 6c) with the amplification rate where b_0 is semiquantitatively approximated by the extrapolated bioluminescence intensity at $t = 0$ and approximated $p_\infty/p_0 \approx p_{\text{stock}}/p_0$ (ordinate, Suppl. Fig. 6c). We found a clear correlation between both quantities (Pearson r=0.67, p=10^{-44}) and therefore performed more replicate experiments (five per condition) using the much less laborious approximation of phage amplification rate (x-axis) for full characterization (Fig. 4e-f). It should be noted that while the Coulter counter provides a quantitative readout of bacterial concentration, bioluminescence provides only a semi-quantitative readout of bacterial concentration. However, this is sufficient for measuring antibiotic-dependent changes in amplification rate.

References

1. Dion, M. B., Oechslin, F. & Moineau, S. Phage diversity, genomics and phylogeny. *Nat. Rev. Microbiol.* **18**, 125–138 (2020).
2. Abedon, S. T. Automating Predictive Phage Therapy Pharmacology. *Antibiotics* **12**, 1423 (2023).
3. Abedon, S. T. How Simple Maths Can Inform Our Basic Understanding of Phage Therapy. *Clin. Infect. Dis.* **77**, S401–S406 (2023).
4. Lindberg, H. M., McKean, K. A. & Wang, I.-N. Phage fitness may help predict phage therapy efficacy. *Bacteriophage* **4**, e964081 (2014).
5. Pirnay, J.-P. *et al.* Personalized bacteriophage therapy outcomes for 100 consecutive cases: a multicentre, multinational, retrospective observational study. *Nat. Microbiol.* 1–20 (2024) doi:10.1038/s41564-024-01705-x.
6. Kropinski, A. M., Mazzocco, A., Waddell, T. E., Lingohr, E. & Johnson, R. P. Enumeration

of bacteriophages by double agar overlay plaque assay. *Methods Mol. Biol. Clifton NJ* **501**, 69–76 (2009).

7. Geng, Y., Nguyen, T. V. P., Homaee, E. & Golding, I. Using population dynamics to count bacteriophages and their lysogens. 2023.10.06.561271 Preprint at https://doi.org/10.1101/2023.10.06.561271 (2023).
8. Dharmaraj, T. *et al.* Rapid assessment of changes in phage bioactivity using dynamic light scattering. *PNAS Nexus* **2**, pgad406 (2023).
9. Kropinski, A. M. Practical Advice on the One-Step Growth Curve. in *Bacteriophages* (eds. Clokie, M. R. J., Kropinski, A. M. & Lavigne, R.) vol. 1681 41–47 (Springer New York, New York, NY, 2018).
10. Nabergoj, D., Modic, P. & Podgornik, A. Effect of bacterial growth rate on bacteriophage population growth rate. *MicrobiologyOpen* **7**, e00558 (2018).
11. Styles, K. M., Brown, A. T. & Sagona, A. P. A Review of Using Mathematical Modeling to Improve Our Understanding of Bacteriophage, Bacteria, and Eukaryotic Interactions. *Front. Microbiol.* **12**, 724767 (2021).
12. Konopacki, M., Grygorcewicz, B., Dołęgowska, B., Kordas, M. & Rakoczy, R. PhageScore: A simple method for comparative evaluation of bacteriophages lytic activity. *Biochem. Eng. J.* **161**, 107652 (2020).
13. Storms, Z. J., Teel, M. R., Mercurio, K. & Sauvageau, D. The Virulence Index: A Metric for Quantitative Analysis of Phage Virulence. *PHAGE* **1**, 27–36 (2020).
14. Rajnovic, D., Muñoz-Berbel, X. & Mas, J. Fast phage detection and quantification: An optical density-based approach. *PLOS ONE* **14**, e0216292 (2019).
15. Keith, M. *et al.* Predictive phage therapy for Escherichia coli urinary tract infections: Cocktail selection for therapy based on machine learning models. *Proc. Natl. Acad. Sci.* **121**, e2313574121 (2024).
16. Gencay, Y. E. *et al.* Engineered phage with antibacterial CRISPR–Cas selectively reduce E. coli burden in mice. *Nat. Biotechnol.* **42**, 265–274 (2024).
17. Blazanin, M., Vasen, E., Jolis, C. V., An, W. & Turner, P. E. Theoretical validation of

growth curves for quantifying phage-bacteria interactions. 2023.06.29.546975 Preprint at https://doi.org/10.1101/2023.06.29.546975 (2023).

18. Bulssico, J., Papukashvili, I., Espinosa, L., Gandon, S. & Ansaldi, M. *Phage-Antibiotic Synergy: Cell Filamentation Is a Key Driver of Successful Phage Predation*. http://biorxiv.org/lookup/doi/10.1101/2022.11.28.518157 (2022) doi:10.1101/2022.11.28.518157.

19. Maffei, E. *et al.* Systematic exploration of Escherichia coli phage–host interactions with the BASEL phage collection. *PLOS Biol.* **19**, e3001424 (2021).

20. Kavčič, B., Tkačik, G. & Bollenbach, T. Mechanisms of drug interactions between translation-inhibiting antibiotics. *Nat. Commun.*

21. Nabergoj, D., Modic, P. & Podgornik, A. Effect of bacterial growth rate on bacteriophage population growth rate. *MicrobiologyOpen* **7**, e00558 (2018).

22. Kebriaei, R. *et al.* Optimization of Phage-Antibiotic Combinations against Staphylococcus aureus Biofilms. *Microbiol. Spectr.* **11**, e04918-22.

23. Kever, L. *et al.* Aminoglycoside Antibiotics Inhibit Phage Infection by Blocking an Early Step of the Infection Cycle. *mBio* **13**, e00783-22 (2022).

24. Stachurska, X., Roszak, M., Jabłońska, J., Mizielińska, M. & Nawrotek, P. Double-Layer Agar (DLA) Modifications for the First Step of the Phage-Antibiotic Synergy (PAS) Identification. *Antibiotics* **10**, 1306 (2021).

25. Mitarai, N., Brown, S. & Sneppen, K. Population Dynamics of Phage and Bacteria in Spatially Structured Habitats Using Phage λ and Escherichia coli. *J. Bacteriol.* **198**, 1783–1793 (2016).

26. Piel, D. *et al.* Phage–host coevolution in natural populations. *Nat. Microbiol.* **7**, 1075–1086 (2022).

27. Göller, P. C. *et al.* Multi-species host range of staphylococcal phages isolated from wastewater. *Nat. Commun.* **12**, 6965 (2021).

28. Kauffman, K. M. *et al.* Resolving the structure of phage–bacteria interactions in the context of natural diversity. *Nat. Commun.* **13**, 372 (2022).

29. Gelman, D. *et al.* Clinical Phage Microbiology: a suggested framework and recommendations for the in-vitro matching steps of phage therapy. *Lancet Microbe* **2**, e555–e563 (2021).

30. Gaborieau, B. *et al.* Predicting phage-bacteria interactions at the strain level from genomes. 2023.11.22.567924 Preprint at https://doi.org/10.1101/2023.11.22.567924 (2023).

31. Lood, C., Haas, P.-J., van Noort, V. & Lavigne, R. Shopping for phages? Unpacking design rules for therapeutic phage cocktails. *Curr. Opin. Virol.* **52**, 236–243 (2022).

32. Guerrero-Bustamante, C. A., Dedrick, R. M., Garlena, R. A., Russell, D. A. & Hatfull, G. F. Toward a Phage Cocktail for Tuberculosis: Susceptibility and Tuberculocidal Action of Mycobacteriophages against Diverse Mycobacterium tuberculosis Strains. *mBio* **12**, e00973-21.

33. Gerovac, M. *et al.* Phage proteins target and co-opt host ribosomes immediately upon infection. *Nat. Microbiol.* **9**, 787–800 (2024).

34. Dos Santos, C., Dos Santos, L. S. & Franco, O. L. Fosfomycin and nitrofurantoin: classic antibiotics and perspectives. *J. Antibiot. (Tokyo)* **74**, 547–558 (2021).

35. Chevallereau, A., Pons, B. J., van Houte, S. & Westra, E. R. Interactions between bacterial and phage communities in natural environments. *Nat. Rev. Microbiol.* **20**, 49–62 (2022).

36. Borin, J. *et al.* Rapid bacteria-phage coevolution drives the emergence of multiscale networks. *Science* doi:10.1126/science.adi5536.

37. Scott, M. & Hwa, T. Shaping bacterial gene expression by physiological and proteome allocation constraints. *Nat. Rev. Microbiol.* **21**, 327–342 (2023).

Acknowledgments

We thank Alexander Harms for sharing the BASEL collection; Gerrit Ansmann, Theresa Fink, Michael Lässig, and Rob Lavigne for feedback on the manuscript; and the entire Bollenbach group for fruitful discussions. This work was supported in part by German Research Foundation (DFG) Collaborative Research Centre (SFB) 1310. Y.M. was supported by a Marie Curie Fellowship from the European Union. Fig. 2c was created with Biorender.com.

Author contributions

Conceptualisation: Y.M. and T.B.; Investigation: Y.M., J.M., D.T.; Mathematical model: D.T., Y.M.; Writing original draft: Y.M.; writing - review and editing: Y.M. J.M., D.T., T.B.; Supervision: T.B.; Funding acquisition: T.B.

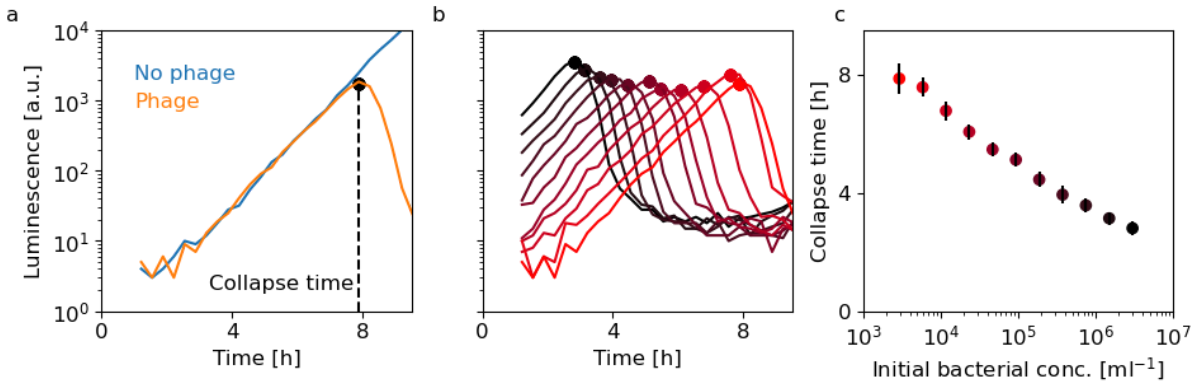

Fig. 1 Phage-induced bacterial population collapse is limited by phage-bacteria adsorption. a) Exemplary growth curve of *E. coli* in the absence and presence of a phage (Bas04), measured by bioluminescence (Methods). **b)** Growth curves measured at different initial bacterial concentrations b_0 (3×10^3 - 3×10^6 ml^{-1} from red to black; colors as in c) at a fixed multiplicity of infection (MOI, i.e. phage-to-bacteria ratio) of 0.4. **c)** Collapse times from **b** ; the observed logarithmic decrease (Pearson's $\rho=0.995$, $p=10^{-10}$) suggests that the phage-amplification kinetics is adsorption-limited (Supplementary Information). Error bars show standard errors from bootstrapping the growth curves.

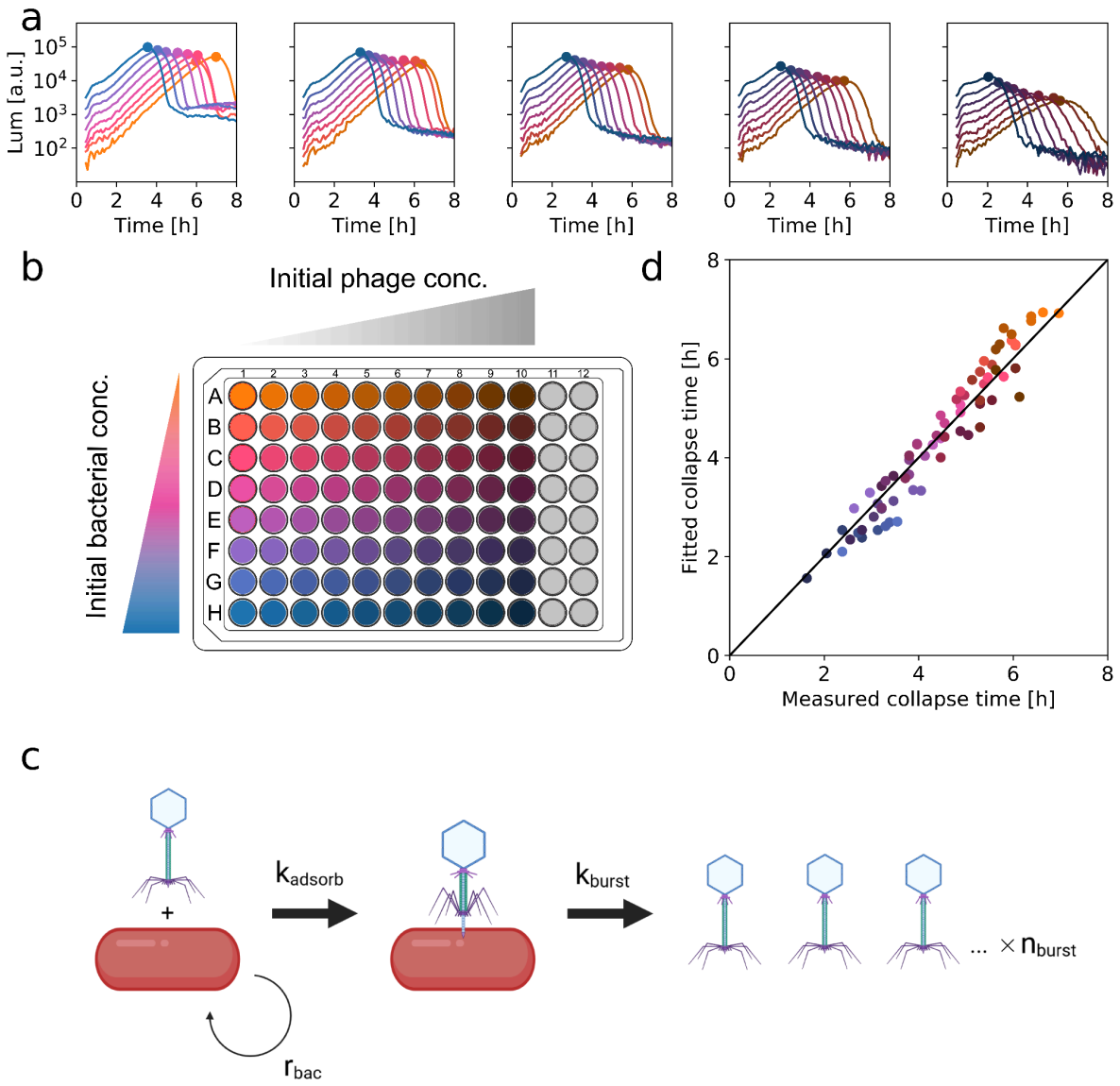

Fig. 2 A mathematical model of phage infection allows the extraction of key phage amplification parameters (PHORCE). a–b) *E. coli* growth curves measured by bioluminescence (Methods) in the presence of the phage Bas04 at all combinations of eight different initial bacterial concentrations (1.1×10^4 – 1.4×10^6 ml^{-1}, orange to blue) and ten different initial phage concentrations (2.5×10^3 – 1.3×10^6 ml^{-1}, light to dark). Due to the large number of growth curves, only every other phage concentration is shown. Circles indicate the collapse points. **c)** Schematic of minimal model of phage amplification (Supplementary Information). We approximate the process by a single parameter: The phage amplification rate $r_{\mathrm{pha}} = n_{\mathrm{burst}} k_{\mathrm{adsorb}}$. **d)** Comparison of observed collapse times and collapse times from the model. Using Eq. 1, we fit all collapse times measured in panel **a** simultaneously with a single value of r_{pha} as the only free parameter; the model is consistent with the experimental data (r^2=0.93).

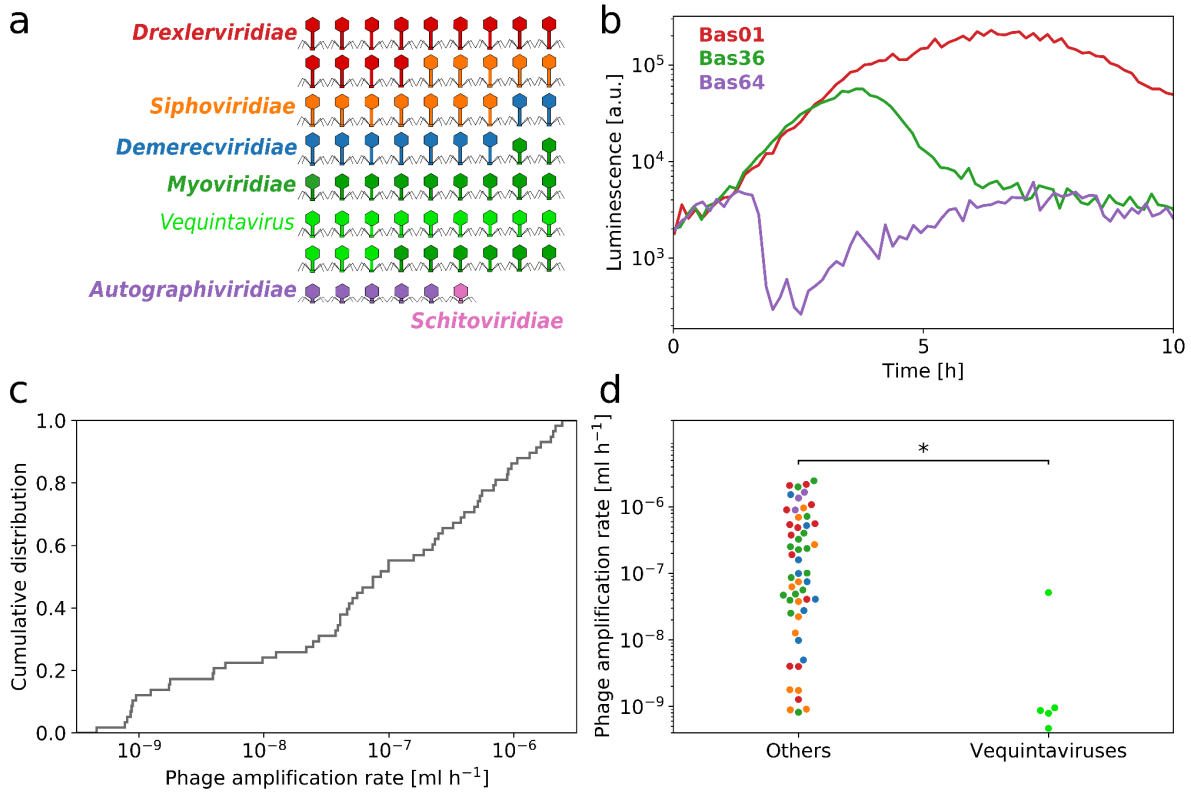

Fig. 3 High-throughput PHORCE reveals an extremely wide range of phage amplification rates for a collection of diverse lytic phages. a) Schematic of 69 phages in the BASEL collection showing the phage morphology and taxonomic classification (colors). **b)** Example growth curves in the presence of different phages (colors) at the same initial phage (1×10^5 ml^{-1}) and bacterial concentration (4×10^5 ml^{-1}) with different collapse times. **c)** Distribution of the phage amplification rates for the entire BASEL collection (Methods). **d)** Vequintavirus members have a significantly lower amplification rate ($p=3\times10^{-6}$, Mann–Whitney *U* test) than other phages. The detection limit for the phage amplification rate was 3×10^{-10} ml h^{-1}, as slower growing phages did not cause a collapse within the exponential growth regime of the bacteria. This was the case for 7 of 12 vequintavirus members and 4 of 57 others; these phages were excluded from the analysis.

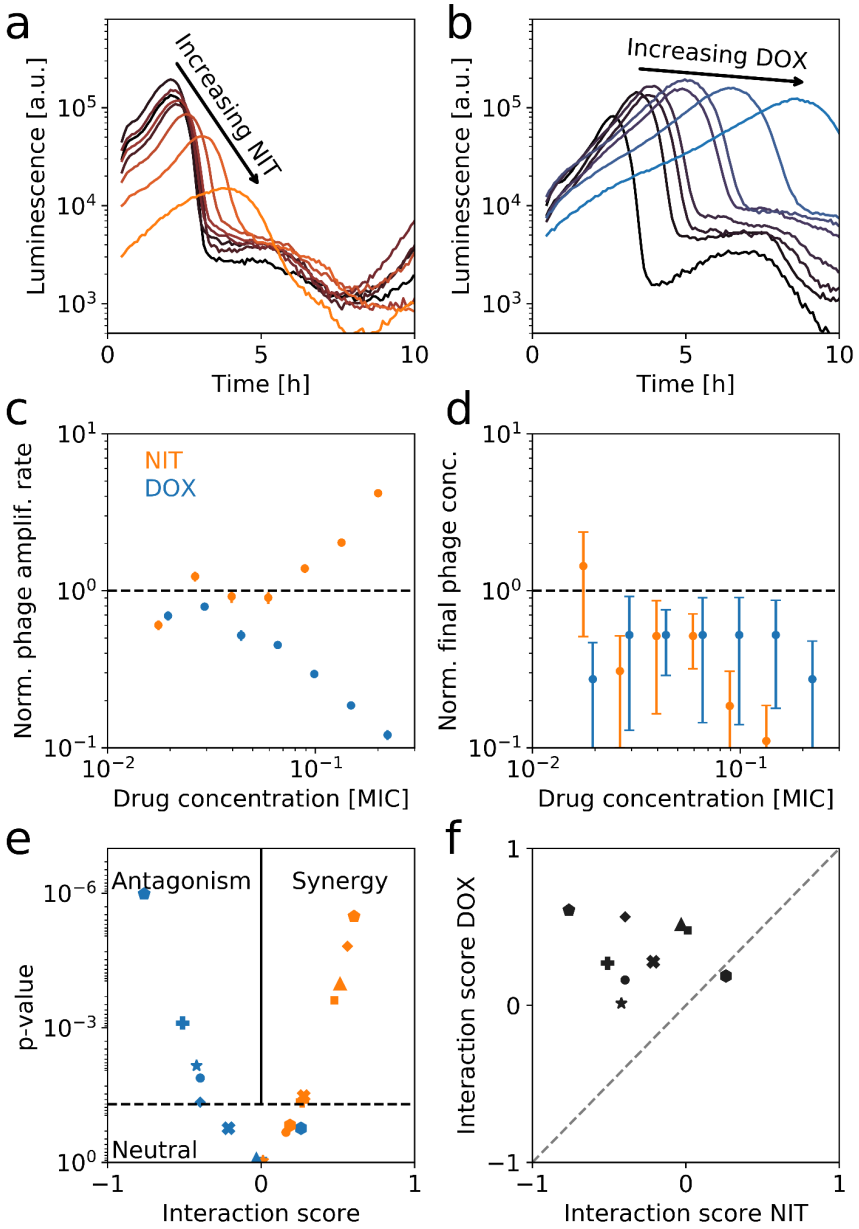

Fig. 4 Phage-antibiotic interactions are determined by the antibiotic, not the phage. a–b) Growth curves of bacteria and phages (Bas04) in the presence of nitrofurantoin (**a**) and doxycycline (**b**). **c)** Phage amplification rate of Bas04 at different concentrations of nitrofurantoin (orange) and doxycycline (blue). While the phage amplification rate increases with nitrofurantoin (synergy), it decreases with doxycycline (antagonism). Error bars show propagated standard errors from bootstrapping the growth curves (typically smaller than the marker size). **d)** As **c**, but for phage yield (Methods). In contrast to the phage amplification rate, the yield is not markedly different between the two drugs. Error bars show propagated standard errors from bootstrapping the growth curves. **e)** Interaction score of nine different phages with both nitrofurantoin (orange) and doxycycline (blue); interaction score is defined as Kendall's τ of the antibiotic-dependent phage amplification rate (as in **c**). The dashed line is at p=0.05; positive correlations indicate synergy, negative values indicate antagonism. Nitrofurantoin shows significantly more synergistic interactions than doxycycline (p=0.008, Wilcoxon test signed rank test). **f)** Scatterplot comparing interaction scores of different

phages with nitrofurantoin to those with doxycycline. No correlation was found between the two drugs (p=0.9, Kendalls τ), showing that the antibiotic, but not the phage, is predictive of the interaction. Dashed line indicates identity. Phages in **e,f**: Bas01 (■); Bas04 (●); Bas10 (**+**); Bas14 (⬢); Bas23 (×); Bas30 (★); Bas37 (⬟); Bas42 (♦); Bas63 (▲).

Supplementary Information

Model of phage amplification kinetics

Adsorption-limited regime

Phage amplification kinetics are modeled as a two-step process: Phages must first adsorb to bacteria at a rate k_{adsorb}, after which they cause lysis of bacteria at a rate k_{burst} (inverse latent period). With each cycle, n_{burst} phages are created and one bacterium disappears. We first consider the adsorption-limited regime ($k_{\mathrm{adsorb}} b \ll k_{\mathrm{burst}}$). Together with the bacterial growth rate r_{bac}, we express the dynamics of the bacterial ($b(t)$) and phage ($p(t)$) concentrations as:

$$\frac{\mathrm{d}b}{\mathrm{d}t} = r_{\mathrm{bac}} b(t) - k_{\mathrm{adsorb}} p(t) b(t) \qquad \text{(Suppl. Eq. 1a)}$$

$$\frac{\mathrm{d}p}{\mathrm{d}t} = n_{\mathrm{burst}} k_{\mathrm{adsorb}} p(t) b(t) \qquad \text{(Suppl. Eq. 1b)}$$

The condition for the collapse time of the bacterial population is that the bacterial death rate due to the phage is equal to the growth rate of the bacteria, which implies that the collapse time is implicitly given by:

$$p(t_{\mathrm{col}}) = \frac{r_{\mathrm{bac}}}{k_{\mathrm{adsorb}}}. \qquad \text{(Suppl. Eq. 2)}$$

Next, we calculate the collapse time of the bacterial population by neglecting the phage contribution in (Suppl. Eq. 1a). In this approximation: $b(t) = b_0 \mathrm{e}^{r_{\mathrm{bac}} t}$.

For a known initial bacterial concentration b_0, we can obtain the phage concentration as a function of time by integrating (Suppl. Eq. 1b). In this regime, the phage population grows super-exponentially from its initial value p_0:

$$p(t) = p_0 \mathrm{e}^{\frac{n_{\mathrm{burst}}}{r_{\mathrm{bac}}} k_{\mathrm{adsorb}} b_0 (\exp(r_{\mathrm{bac}} t) - 1)}. \qquad \text{(Suppl. Eq. 3)}$$

We then insert in the collapse condition (Suppl. Eq. 2) and solve for t_{col}, to obtain

$$t_{\mathrm{col}} = \frac{1}{r_{\mathrm{bac}}} \log\left(1 + \frac{r_{\mathrm{bac}}}{k_{\mathrm{adsorb}} n_{\mathrm{burst}} b_0} \left(\log\left(\frac{r_{\mathrm{bac}}}{p_0\, k_{\mathrm{adsorb}}}\right)\right)\right). \qquad \text{(Suppl. Eq. 4)}$$

We define the phage amplification rate as $r_{\mathrm{pha}} = n_{\mathrm{burst}} k_{\mathrm{adsorb}}$ and eliminate the dependence on k_{adsorb} by approximating the phage concentration at the onset of collapse as $p(t_{\mathrm{col}}) = \frac{r_{\mathrm{bac}}}{k_{\mathrm{adsorb}}} \approx p_\infty$, with the final phage concentration p_∞ (phage yield) to obtain the collapse time in (Eq. 1):

$$t_{\mathrm{col}} = \frac{1}{r_{\mathrm{bac}}} \log\left(1 + \frac{r_{\mathrm{bac}}}{r_{\mathrm{pha}} b_0} \log\left(\frac{p_\infty}{p_0}\right)\right). \qquad \text{(Suppl. Eq. 5)}$$

Finally, we use the measured collapse time to infer the phage amplification rate by solving (Suppl. Eq. 5) for r_{pha}:

$$r_{\mathrm{pha}} = \frac{r_{\mathrm{bac}}}{b_0\left(\mathrm{e}^{r_{\mathrm{bac}} t_{\mathrm{col}}} - 1\right)} \log\left(\frac{p_\infty}{p_0}\right). \qquad \text{(Suppl. Eq. 6)}$$

We find good agreement between this model and the experimental data (Fig. 2d, Suppl. Fig. 4b).

Bursting-limited regime

So far, we have considered the adsorption-limited regime where $k_{\mathrm{adsorb}} b(t) \ll k_{\mathrm{burst}}$. We now consider the opposite regime, where bursting is limiting:

$$\frac{\mathrm{d}b}{\mathrm{d}t} = r_{\mathrm{bac}} b(t) - p(t) k_{\mathrm{burst}} \qquad \text{(Suppl. Eq. 7)}$$

$$\frac{\mathrm{d}p}{\mathrm{d}t} = p(t) n_{\mathrm{burst}} k_{\mathrm{burst}} \qquad \text{(Suppl. Eq. 8)}$$

In this regime, the dynamics can be solved analytically, yielding

$$b(t) = b_0 e^{r_{\mathrm{bac}} t} - \frac{k_{\mathrm{burst}} p_0 \left(e^{k_{\mathrm{burst}} n_{\mathrm{burst}} t} - e^{r_{\mathrm{bac}} t}\right)}{k_{\mathrm{burst}} n_{\mathrm{burst}} - r_{\mathrm{bac}}} \qquad \text{(Suppl. Eq. 7)}$$

$$p(t) = p_0 \mathrm{e}^{n_{\mathrm{burst}} k_{\mathrm{burst}} t} \qquad \text{(Suppl. Eq. 8)}$$

Next, we calculate the collapse time ($\mathrm{d}b/\mathrm{d}t|_{t=t_{col}} = 0$). We find that the population collapses at a fixed multiplicity of infection ($\mathrm{MOI} = p/b$):

$$p_{\mathrm{col}}/b_{\mathrm{col}} = \mathrm{MOI}_{\mathrm{col}} = r_{\mathrm{bac}}/k_{\mathrm{burst}} \qquad \text{(Suppl. Eq. 9)}$$

Imposing the collapse condition we obtain for the collapse time:

$$t_{\mathrm{col}} = \frac{\log\left(\frac{r_{\mathrm{bac}}}{k_{\mathrm{burst}}}\left(\frac{1}{n_{\mathrm{burst}}} + \frac{1}{\mathrm{MOI}_0} - \frac{r_{\mathrm{bac}}}{k_{\mathrm{burst}}}\right)\right)}{k_{\mathrm{burst}} n_{\mathrm{burst}} - r_{\mathrm{bac}}} \qquad \text{(Suppl. Eq. 11)}$$

Therefore, we find that the collapse time in the bursting limited regime depends only on the initial MOI, and not on the absolute phage and bacterial concentrations separately. This result is inconsistent with the experimental results in Fig. 1c and Suppl. Fig. 4a, as both show a monotonic decrease in collapse time as a function of the initial bacterial concentration at a fixed initial MOI. In principle, the experimental system could be in the intermediate regime where $k_{\mathrm{adsorb}} b(t)$ is on the order of k_{burst} for at least for some duration of the experiment. However, our experimental results indicate that this situation can only occur relatively late (if at all), in the last few infection cycles before the collapse. The fact that

the adsorption-limited case (Suppl. Eq. 5) already shows good agreement with the experimental data (Fig. 2d, Suppl. Fig. 4b) supports that it captures the essence of the dynamics up to the collapse and is thus sufficient as a minimal model. Therefore, we do not consider more complex models with inherently more free parameters.

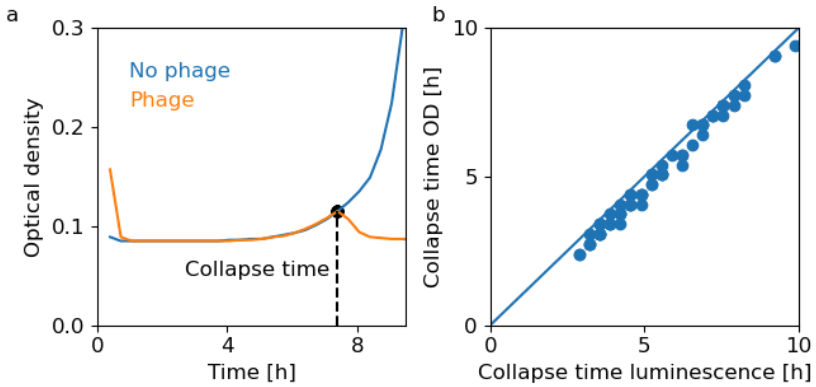

Suppl. Fig. 1 Comparison of collapse times obtained from bioluminescence and optical density measurements. a) Example of an *E. coli* growth curve in the absence (blue) and presence (orange) of a phage (Bas04), as measured by optical density (Methods). Initially there was condensation on the lid of the 96-well plate, resulting in an artifactually higher optical density for the first half hour. **b)** The collapse time of phage Bas04 measured with both bioluminescence and optical density for the same samples. All combinations of 7 MOIs (0.0004 – 0.3, 3× steps) and 11 bacterial concentrations (3×10^3 – 3×10^6, 2× steps) were measured. Both methods show close agreement (Pearson's $\rho=0.99$, $p=10^{-65}$).

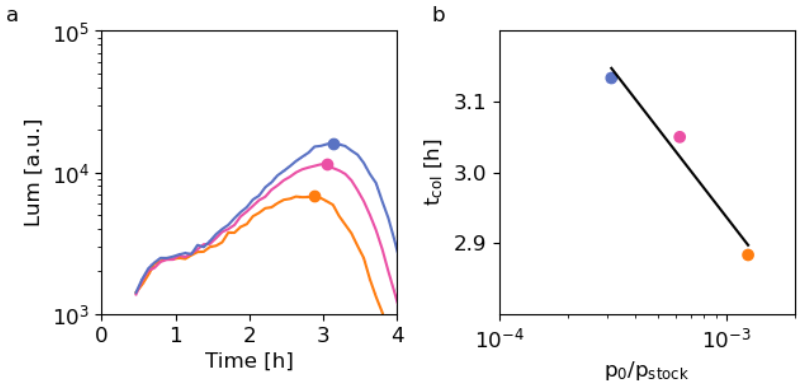

Suppl. Fig. 2 Calculation of the phage concentration from growth curves. a) Bacterial growth curves were measured in the presence of several different dilutions (1/800, 1/1600 and 1/3200, respectively orange, pink and blue) of the Bas04 phage stock used in Figs. 1 and 2 at a fixed initial bacterial concentration (4×10^5 ml^{-1}) to quantify the phage concentration-dependent collapse time. **b)** We fit these collapse times (t_{col}) with a logarithmic decay (black line, see Ref. [7] for details) to obtain a calibration curve that we use to determine unknown phage concentrations in samples containing the phage Bas04.

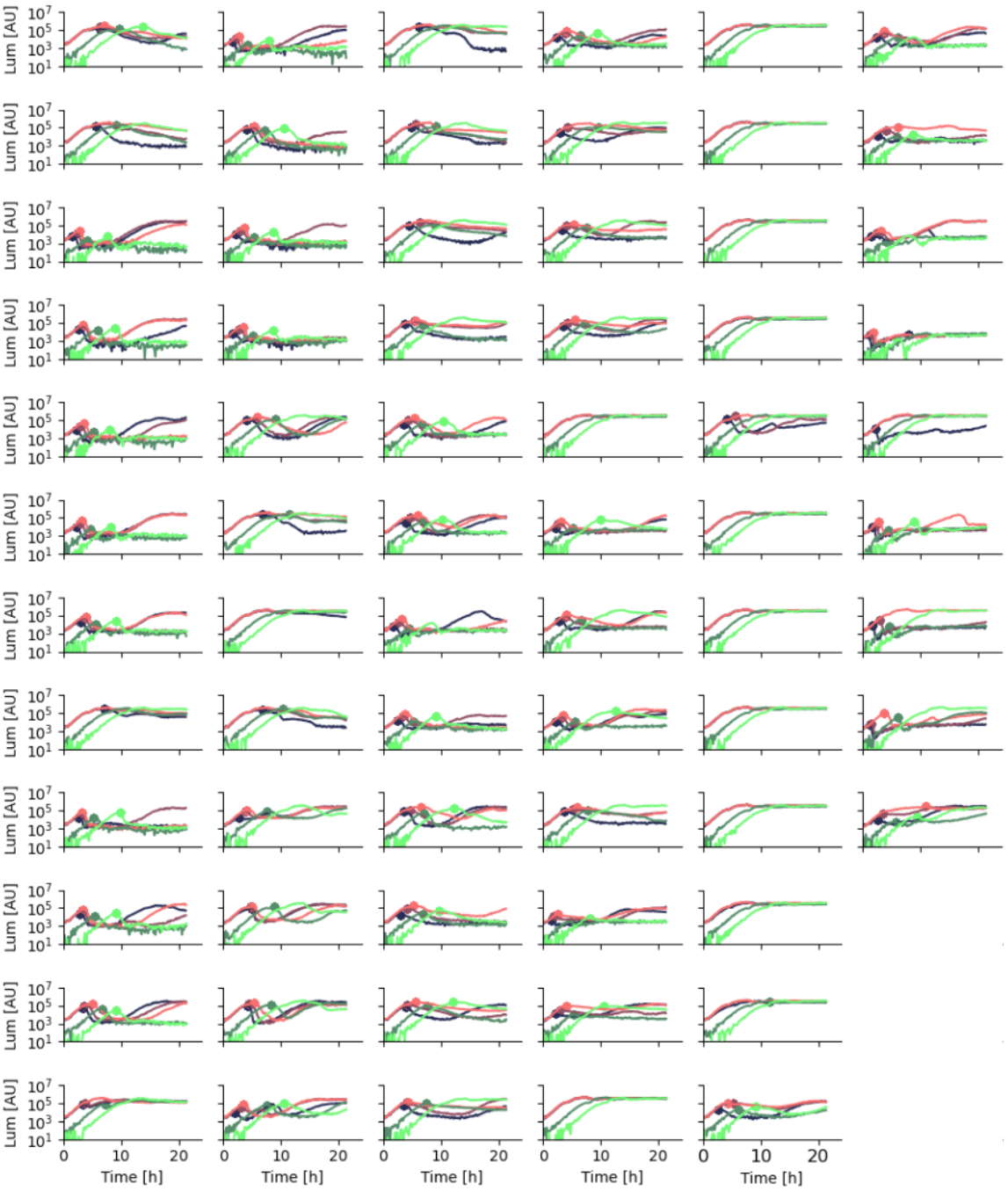

Suppl. Fig. 3 Raw bacterial growth curves in the presence of the BASEL phages. Each graph shows a time-resolved bacterial growth curve, measured using bioluminescence (Methods), in the presence of a different phage. Green to black shows different initial bacterial concentrations (resp. 480, 1.44×10^4 and 4.32×10^5 ml^{-1}) at a fixed initial MOI and red to black shows different phage concentrations at a fixed initial bacterial concentration (resp. 8.1×10^5, 2.7×10^4 and 900× diluted from the phage stock solutions). The first column shows the BASEL phages 1–12, the second column shows 13–24, and so on (top to bottom).

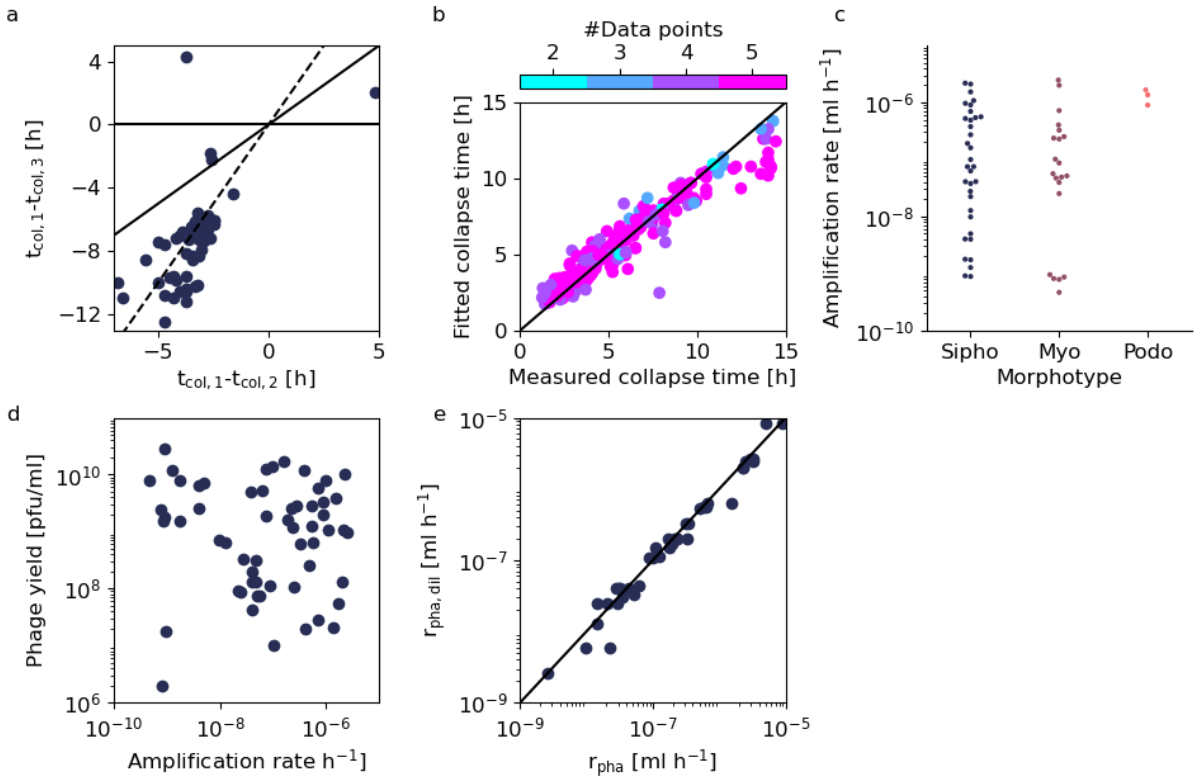

Suppl. Fig. 4 Phage amplification characteristics of the BASEL collection. Analysis of the growth curves in Suppl. Fig. 3. **a)** The collapse time was measured at three bacterial densities, keeping the ratio of phages to bacteria (multiplicity of infection, MOI) fixed, for the entire BASEL collection. $t_{\mathrm{col},1-3}$ indicate time of collapse at resp. the lowest, middle and highest bacterial density. Each data point represents a different phage. All data points below the two solid lines show a monotonic increase in collapse time as a function of the bacterial concentration. The dashed line indicates where the collapse time increases with the logarithm of the bacterial concentration. The vast majority of data points lie below the two solid lines and cluster around the dashed line, suggesting that the amplification kinetics of all BASEL phages are predominantly adsorption-limited. **b)** The fitted and measured collapse times for all BASEL phages, similar to Fig. 2d, show good agreement (Pearson's ρ=0.95, p=10^{-129}), regardless of the number of fitted data points (color). **c)** Phage amplification rates for different phage morphotypes, 3/6 podoviruses, 0/34 siphoviruses and 8/29 myoviruses had a phage amplification rate below the detection limit (3×10^{-10} ml h^{-1}). None of the morphotypes differ significantly from the others (p=0.08, Kruskal-Wallis) and any differences become even more insignificant if the vequintavirus members are excluded from the myoviruses (Fig. 3d, p=0.87, Kruskal-Wallis). **d)** Comparison between the overnight yield (y-axis) and the phage amplification rate (x-axis) for each phage in the BASEL collection shows no significant correlation (τ=-0.04, p=0.6, Kendall rank correlation) **e)** Comparison between the phage amplification rate (x-axis) and its approximation by assuming $p_\infty/p_0 = p_{\mathrm{stock}}/p_0$ (y-axis). Each data point shows the phage amplification rate determined from a single amplification curve (nine phages, three replicates per condition). Both results are in close agreement (Pearson's ρ=0.95, p=10^{-22}).

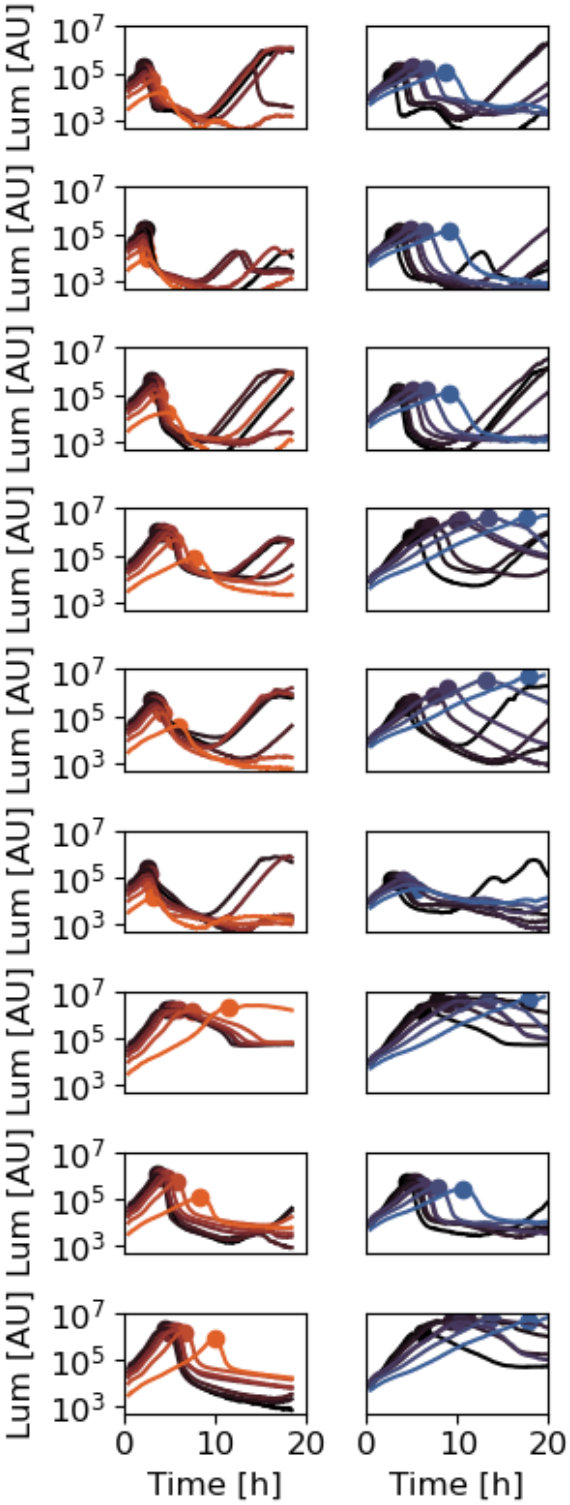

Suppl. Fig. 5 Bacterial growth curves in the presence of antibiotics and phages. Bioluminescence as a function of time. Each row shows a different phage from the BASEL collection (phages from top to bottom: Bas01, Bas04, Bas10, Bas14. Bas17, Bas23, Bas30, Bas37, Bas42, Bas55, Bas63), each column shows a different antibiotic (left: nitrofurantoin, orange; right, doxycycline, blue) at different concentrations (0.02 - 0.2 × MIC from dark to colored, where black is no antibiotic).

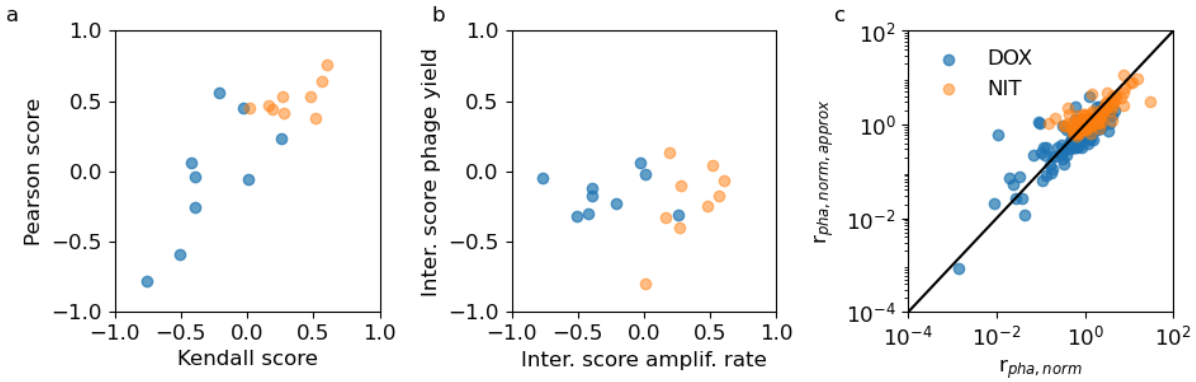

Suppl. Fig. 6 Phage-antibiotic interactions. a) The degree of correlation between the phage amplification rate and the antibiotic concentration was assessed using either a Kendall correlation test (x-axis) or a Pearson correlation test (y-axis). Both scores are significantly correlated with each other (Kendall's τ =0.5, p=0.002). **b)** No correlation was found between the interaction score based on the phage yield and the interaction score based on the amplification rate (p=0.6, Kendall rank correlation). **c)** The phage amplification rate was calculated either by explicitly measuring the initial bacterial concentration and the final phage concentration (x-axis) or by approximating the initial bacterial concentration with the initial bioluminescence value and assuming $p_\infty/p_0 = p_{\mathrm{stock}}/p_0$ (y-axis) (Methods). The explicit and approximate approaches yield similar results (Pearson's ρ=0.67, p=10^{-44}). On both axes, the antibiotic-dependent phage amplification rate was normalized to the phage amplification rate in the absence of the drug. For both doxycycline and nitrofurantoin, nine phages and eight drug concentrations were measured, respectively.